A major purpose of the Technical Information Center is to provide the broadest dissemination possible of information contained in DOE's Research and Development Reports to business, industry, the academic community, and federal, state and local governments.

Although a small portion of this report is not reproducible, it is being made available to expedite the availability of information on the research discussed herein.

LA-UR -89-872

Los Alamos National Laboratory is operated by the University of California for the United States Department of Energy under contract W-7405-ENG-36

LA-UR--89-872

DE89 009387

TITLE SURFACE-BURN MODEL FOR SHOCK INITIATION

AUTHOR(S) Yeh Partom, Jerry Wackerle

SUBMITTED TO Ninth Symposium (International) on Detonation
August 28 - September 1, 1989
Portland, Oregon

DISCLAIMER

Los Alamos Los Alamos National Laboratory
Los Alamos, New Mexico 87545

SURFACE-BURN MODEL FOR SHOCK INITIATION

Yehuda Partom
RAFAEL, P. O. Box 2250
Haifa, Israel

and

Jerry Wackerle
Los Alamos National Laboratory
Los Alamos, NM 87545

An investigation of a surface-burn model of the shock-induced decomposition, initiation and detonation of heterogeneous explosives is described. The model assumes a microscale process with hot spots ignited by viscoplastic heating at the boundaries of collapsing pores. A relatively thin reaction zone, or burn surface, is driven by the conduction of the heat of reaction, and has a surface-burn velocity with an Arrhenius dependence on the temperature of the unreacted solid component. Global reaction rates are derived from the microscale model with an empirical burning topology function and a macroscopic reactant-product mixture defined by pressure equilbrium, ideal mixing of specific volume and internal energy, and isentropic response of the unreacted constituents. With simplifying assumptions, the model is extended to treat multi-component explosives. The model is implemented into a method of characteristics hydrocode and shown to be effective in simulating several examples of initiation experiments on TATB explosives.

INTRODUCTION

Many reaction-rate correlations and models have been proposed and used for the numerical hydrodynamic simulation of the shock initiation and detonation of heterogeneous explosives; a comprehensive review of such models is provided by Reference 1. Most models can be included in two broad categories: bulk (or bulk-like) reaction and surface burning. Here we describe an investigation with a specific surface-burn model.

The foundations of the model were presented at the Seventh Symposium on Detonation.[2] That study treated the growth of hot spots as a moving decomposition front (surface), with a burn velocity depending only on the temperature of the unreacted solid phase.

Here we report a project at Los Alamos to extend and refine the model. First, we developed the set of equations needed to implement the model in a method of characteristics hydrocode SHIN.[1] We did the same for a bulk reaction model and for a mixed, simultaneously occurring surface-burn/bulk-reaction model. By applying both models to the reaction zone for steady detonation, we were able to conclude that surface burn is dominant and appropriate. A more general burning topology function was developed to connect the burning velocity and microscopic reaction history. We calibrated the surface burn model for TATB and used SHIN to simulate different kinds of initiation situations, such as sustained shock, short shock, ramp loading, different densities (porosities), and different initial temperatures.[3]

We then extended the model to multicomponent materials.[4] This enabled us to simulate the initiation process of explosive formulations from the response of their components. We were also able to model the initiation of explosives with grain-size distributions and applied this to simulate the experimentally-observed crossover in reaction-rate effect for granular TATB.[5]

In a related investigation, we examined the so-called shell model and were able to show that viscoplastic heating, upon pore collapse, is an appropriate hot-spot ignition mechanism for our surface-burn model.[6]

In the following, we describe the physical picture behind our surface-burn model. We then outline the model and the flow equations needed in our method of characteristics code. Finally we present some examples of results with the model.

PHYSICAL PICTURE

We assume that reaction of heterogeneous explosives under prompt pressure loading starts at hot spots on ir

ignition sites. We further assume that these hot spots are related to pores in the explosive, and that ignition is triggered by viscoplastic heating during collapse of the pores.

The collapse and viscoplastic heating of pores was modeled in spherical geometry by Carrol and Holt[7], and has been used by a number of authors to model hot spots in shocked explosives.[8-12] In Reference 6 we reexamined viscoplastic pore-collapse to see if it is an adequate mechanism for hot-spot ignition for the surface-burn growth model described below. For TATB we found that, above 2 GPa and after about 30 ns of inward motion, the pore boundary heats up to above 2000 K, sufficient to start fast reaction there. Within 1 ns the cavity is filled with hot-reaction products of at least 3500 K.

In Reference 2, we found that if threshold conditions outlined below are met, this hot gas in the cavity would drive a reaction process into the unreacted grains around the cavity. To investigate this growth mechanism, we set up a heat-conduction, chemical-kinetics problem in spherical symmetry. We ignored the influence of pressure fluctuations much as in the ignition pore collapse model, assuming that pressure equilibration by wave reverberations is a much faster process. Solving the steady-state kinetics problem (and corroborating the results with time-dependent calculations)[2], we obtained a physical picture for the growth of reaction from hot spots. Whenever the cavity size is above a critical value d_{cr}, and the gas temperature in the cavity is above a critical value T_{cr}, a steady outgoing reaction zone develops.

The analyses[2] shows that the reaction zone is very thin compared to the cavity size, and can be regarded as a moving reaction surface. We call it a burning surface. The rather unusual conclusion of the analysis is that this burning surface propagates with a velocity V_H which depends only on the temperature of the unreacted material ahead of the surface, T_s. It does not depend on the temperature in the gas as long as the critical conditions are met. The critical temperature is given by:

$$T_{cr} = T_s + \frac{Q}{C_p} \sim T_s + 2000\ K \qquad (1)$$

where Q is the heat of reaction and C_p the heat capacity. The critical size d_{cr} also is a function of T_s, with d_{cr} decreasing with increasing T_s.

The burn surface velocity V_H can be calculated from the steady state, heat-conduction, chemical-kinetics problem. In Reference 2, thermal kinetics information was used for PETN, and we found that $V_H(T_s)$ for that explosive can be represented by an Arrhenius form,

$$V_H = Z_H e^{-T_H/T_s} \qquad (2)$$

where T_H is of the order of 5000 K. We assume that this would hold for other explosives as well. As generally reliable data on the chemical kinetics of explosives are not available, in the present study we regard Z_H and T_H as material parameters to be calibrated from shock initiation experiments.

From the burn-surface velocity and topology one can calculate the reaction rate. The burn surfaces have a very complex geometry that becomes even more complex as adjacent burn surfaces coalesce. In Reference 2, we used a geometric construction appropriate for a spherical, "hot-burning" topology, but subsequent work showed serious limitations with that form.[13] In the present work we regard the average burn-surface topology as a material function to be calibrated from experiments. We define a dimensionless Burn-Topology Function (BTF), $y(\lambda)$, such that

$$\dot{\lambda} = y(\lambda)\frac{V_H}{b/2} \qquad (3)$$

Here λ is the mass fraction of products, the reaction rate $\dot{\lambda}$ is the Lagrangian (material) time derivative of this quantity, and b is the average cell size or mean distance between hot spots, which can be approximated by the average grain size. A schematic profile of $y(\lambda)$ is shown in Figure 1. The left part of the curve is related to hole (outgoing) burning while the right part is mainly grain (ingoing) burning.

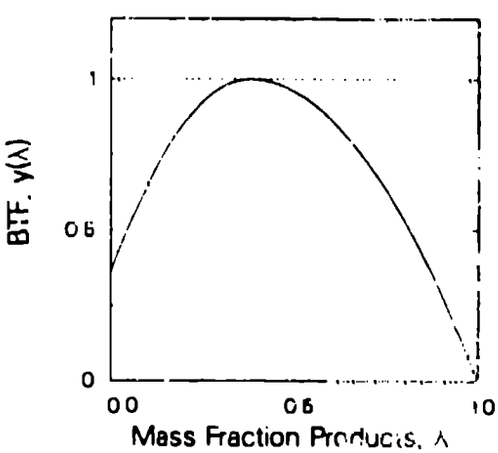

FIGURE 1. SCHEMATIC OF THE BURNING TOPOLOGY FUNCTION.

For high enough temperatures, it is plausible to assume that bulk reaction would occur in the grains outside the moving burn surfaces, as shown schematically in Figure 2. If the rate of bulk reaction is found to be significant, it must be considered simultaneously with the surface burn rate. In such a case we have a double rate problem, which is much more complex, but amenable to analysis.

In Reference 3, we investigated the relative importance of the two rate mechanisms for TATB under shock detonation, an extreme case in terms of the temperature of the unreacted explosive. The investigation compared the integration of the steady state, reactive flow equations through the reaction zone from the von Neumann (VN) spike conditions at the shock front to the Chapman-Jouguet (CJ) state at the end of the reaction. Common

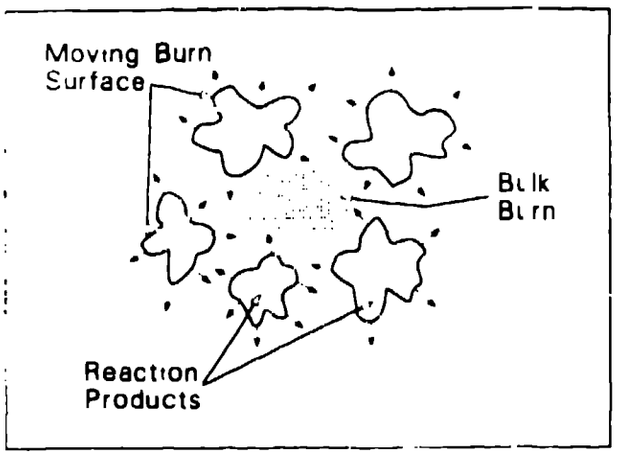

FIGURE 2. SCHEMATIC OF SIMULTANEOUS SURFACE BURN AND BULK REACTION.

to both burn models are the usual assumptions of ideal mixing of specific volumes and internal energies of the unreacted solid and gas products constituents and pressure equilibrium between these two constituents,[1,12–14] as formulated in the next Section. The "isentropic solid" assumption is used with the surface-burn reaction;[12,14] the appropriateness of this choice is discussed below. Also appropriately, thermal equilibrium is assumed between constituents for the bulk burn calculation,[13,14] along with an Arrhenius rate form with constants chosen consistent with reaction-zone measurements on TATB.[5]

Several important conclusions were drawn. For bulk reaction, the reaction-zone thickness is very sensitive to the temperature in the VN state. This temperature cannot be calculated accurately and depends strongly on the initial unshocked state — particularly the porosity — of the explosive. On the other hand, it is known from reaction zone measurements that the detonation reaction-zone thickness is not a sensitive quantity; for different formulations of TATB, it is always of the order of 100 ns.[15] Also, temperature increases rapidly in bulk reaction; even if the initial rate is plausible at some point it increases enormously and the pressure-time $P(t)$ history has an abrupt drop to the CJ point. This has not been observed in reaction zone measurements.[15] In addition, in many cases bulk reaction gave a $P(\lambda)$ dependence through the reaction zone that increased at the VN point before decreasing to CJ conditions. Again, such anomalous behavior has not been observed in reaction-zone measurements. We found that this results from enforcing thermal equilibrium between explosive and products. For small amounts of reaction, the products assume a relatively low temperature imposed by the dominant unreacted explosive. This leads to an initially high gas density and an increasing pressure. On the other hand, using the surface burn model there is no sensitivity to VN temperature and the $P(\lambda)$ curve has the right shape. We concluded that surface burn is the dominant reaction growth mechanism and that simultaneous bulk reaction may be neglected. Nutt reached a similar conclusion.[12]

The macroscopic "mix rules" for the isentropic-solid equation of state are the most appropriate simple representation for the microscopic features of the surface-burning model. The burn surface always separates the unreacted solid from the gaseous products. Heat conduction within the burning surfaces is the driving mechanism for them and already is taken into account by their motion. The unreacted solid is therefore always under adiabatic conditions, and between shocks, under isotropic conditions. Consistent with the microscale level analyses, we assume pressure equilibrium between solid and gas phases on the macroscale level as well, and for the same reason. But there is no temperature equilibrium. The solid and gas phases each has its own temperature as dictated by the microscale analysis. The gas phase is not adiabatic. Newly created products behind the moving burn surfaces are continually added to the existing products in the growing cavities. In our modeling, we assume complete and instantaneous mixing of the products under the constraint of energy conservation. Contrary to the usual approach at Los Alamos,[13–16] we do not derive a pressure-volume-energy-reaction equation of state for the two-phase system in the form $P(V, E, \lambda)$ or $E(P, V, \lambda)$. Instead, we work directly with the separate equations of state of the reactant and products, and calculate the global equation-of-state variables from the mix-rule equations. We believe that in this way we enhance our simulation capacity as we do not need to prepare a new equation of state each time we change the initial conditions of the same explosive. Also contrary to Los Alamos custom,[13–16] we account for the heat of reaction not as a zero-point energy of the gas equation of state, but as an internal heat source. This also adds flexibility to our simulations.

We have used simple equations of state for the solid and gas phases — a Mie-Grüneisen form for the solid, with a constant product of the Grüneisen ratio and density, and, in most cases, a polytropic form for the gas. We are convinced that shock initiation simulation is not sensitive to the type of equations of state of the gas and solid phases. Moreover, differences experienced by using more complex equations of state are, in our opinion, insignificant compared to uncertainties in the reaction rate functions.

The physical picture outlined so far relates to a two-phase system of a simple reactant and its gaseous reaction products. But common explosive formulations consist of more than a single component, where different components are those parts of the explosive that differ in terms of the reaction rate function. Different components in an explosive formulation can be inerts, different explosive materials and different grain size fractions of

the same explosive material. The grain size distribution in common explosive powders is between 10 and 100μm, which Equation (3) shows to be a large factor in reaction rate. To extend our surface-burn model to multicomponent systems and still retain its tractability, we made two approximation which allowed the extension to be made in a relatively straightforward fashion.

First, we assume a common mean equation of state for all the components. To account for a separate equation of state for each of the reactants and products would call for a rederivation of the entire system of equations and restructuring of the solution algorithm. This complication seems unnecessary for calculations such as ours, involving explosives and plastic binders of reasonably similar equations of state, but would be an inappropriate assumption, for example, for metal-loaded explosives.

Second, we ignore interaction among the components in terms of each one of them influencing the BTF of the others. This might not always be a good approximation, as is possible that a fast-reacting component could create additional ignition sites for a slow-reacting component and in this way alter its BTF and its reaction rate. But to account for component interaction one has to take into account the actual microstructural geometry of the multicomponent system, which is beyond the scope of this work.

REACTIVE FLOW EQUATIONS

We outline here the planar reactive-flow equations for an initiation shock building up to a detonation wave and the flow field behind it. Additional shocks through the flow field are not treated.

In terms of the Lagrangian coordinate h and the material time derivative defined earlier, the mass and momentum conservation equations are

$$V - V_o \frac{\partial u}{\partial h} = 0 \quad \text{and} \quad \dot{u} + V_o \frac{\partial P}{\partial h} = 0 \qquad (4)$$

where u is the particle velocity and the sub o denotes the initial (unshocked) state.

To eliminate one of the unknowns, V, u, or P we use the master rate equation[17] in the form

$$V = DP + G\lambda \quad , \qquad (5)$$

derived from energy conservation and differentiation of the mixture equation of state. $E(P, V, \lambda)$. D and G are thermodynamic functions related to the compressibility and thermicity of the explosive, and can be related to similar derivatives of the equations of state $E_s(V_s, P_s)$ and $E_g(P_g, V_g)$ of the solid reactant and gas products. Reference 3 gives these derivations for the assumptions of ideal mixing of specific volume and energy.

$$V = (1 - \lambda)V_s + \lambda V_g \quad \text{and} \quad E = (1 - \lambda)E_s + \lambda E_g \quad , \qquad (6)$$

and pressure equilibrium, and shows the mixture thermodynamic derivative fuctions can be expressed as

$$D = \lambda D_g + (1 - \lambda)D_s$$

and

$$G = \lambda G_g + (1 - \lambda)G_s + V_g - V_s \quad . \qquad (7)$$

With the isentropic solid assumption, we have

$$D_g = \frac{-(\partial E_g/\partial P)}{P + (\partial E_g/\partial V_g)} \quad , \text{ and } D_s = \frac{-(\partial E_s/\partial P)}{P + (\partial E_s/\partial V_s)} \quad ;$$

$$G_g = \frac{Q + E_s - E_g + P(V_s - V_g)}{\lambda[P + (\partial E_g/\partial V_g)]} \text{ and } G_s = 0 \quad . \qquad (8)$$

The reaction rate $\dot{\lambda}$ is given from the surface-burn model Equations (2) and (3). We chose to represent the BTF in Equation (3) by a curve made out of two matching parabolas with a parameter λ_1 that signifies the maximum $(y(\lambda_1) = 1)$ depending on the pressure:

$$y = 4(\lambda + 1/2 - \lambda_1)(1/2 - \lambda + \lambda_1) \quad , \quad \lambda \leq \lambda_1$$

$$y = (1 - \lambda)\frac{1 - 2\lambda_1 + \lambda}{(1 - \lambda_1)^2} \quad , \quad \lambda \geq \lambda_1 \quad , \qquad (9)$$

$$\lambda_1 = \frac{1}{2}(1 - P/P_1) \quad , \quad P_1 \sim 50\text{GPa} \quad .$$

To obtain the equations along characteristic lines, we substitute V from the master rate equation into Equations (4)

$$DP \cdot V_o \frac{\partial u}{\partial h} = -G\dot{\lambda} \text{ and } \dot{u} + V_o \frac{\partial P}{\partial h} = 0 \quad , \qquad (10)$$

which leads to

$$dP + \rho_o C_l\, du + \rho_o^2 C_l^2 G\dot{\lambda} dt = F dt \qquad (11)$$

on

$$\frac{dh}{dt} = \pm C_l \quad . \qquad (12)$$

Here the Lagrangian sound speed C_l is given by

$$C_l^2 = V_o^2/D \quad . \qquad (13)$$

For all other variables (V_g, V_s, E_g, E_s, T_g, T_s), we have differential equations along the Lagrangian path of a form similar to the master rate equation

$$\dot{r} = D_r P + G_r \dot{\lambda} \quad , \qquad (14)$$

where x represents any of these variables. Algorithms for computing D_x, G_x are given in Reference 3.

To integrate along the shock path we use the shock-change equation:

$$\left(\frac{\partial P}{\partial h}\right)_S = \frac{F + (C_L^2/U^2 - 1)\dot{P}}{U(\frac{1}{2}C_H^2/C_L^2 + \frac{1}{2}C_L^2/U^2)} \quad . \qquad (14)$$

where U is the shock velocity, $(dP/dh)_S$ is along the shock path and C_H is defined in terms of the derivative along the Hugoniot curve, $P_H(V)$,

$$C_H^2 = -V_0^2 \frac{dP_H}{dV} \quad . \qquad (15)$$

For steady detonation we use the steady flow condition: $\partial f/\partial h = -\dot{f}/U_D$ for any flow variable f, where U_D is the detonation velocity. The flow equations transform to:

$$V + \frac{V_0}{U_D}\dot{u} = 0 \text{ and } \dot{u} - \frac{V_0}{U_D}\dot{P} = 0 \qquad (16)$$

which leads to

$$\dot{V} + \frac{V_0^2}{U_D^2}\dot{P} = 0 \quad . \qquad (17)$$

which is the equation for the Rayleigh line. Substituting from the inaster rate equation we get:

$$\dot{P} = -\frac{G}{D + V_0^2/U_D^2}\dot{\lambda} = k_p\dot{\lambda} \quad . \qquad (18)$$

so that

$$\frac{\partial P}{\partial \lambda} = k_p(V_0, V_s, P, \lambda) \quad . \qquad (19)$$

which means that one can integrate for $P(\lambda)$ without having to specify the rate function $\dot{\lambda}$.

For a multicomponent system we define a fixed mass fraction ω_i for each component so that $\sum \omega_i = 1$ and a partial degree of reaction λ_i', $(0 \le \lambda_i' \le 1)$, so that $\lambda_i = \omega_i\lambda_i'$. The global mass fraction reacted and reaction rates are thus

$$\lambda = \sum \lambda_i = \sum \omega_i\lambda_i'$$
$$\dot{\lambda} = \sum \dot{\lambda}_i = \sum \omega_i\dot{\lambda}_i' = \sum \omega_i a_i V_{Hi}/(h_i/2) \quad . \qquad (20)$$

The assumptions of an average equation of state and of no interaction between components, as discussed above, allow the details of the multi component model to be incorporated entirely with Equation (20), while retaining the simplicity of a single component formalism in calculating the global reactive hydrodynamic response of the multi component material.

We describe below several examples calculated with the model using the SHIN program.[3,4] This program solves the characteristics relations of Equations (10) to (15) above, in a computational mesh constructed at constant Lagrangian position increments and with the other coordinate taken on pathlines parallel to the shock front. This so-called "Shock Path Net" and the computational algorithms are described in a paper on elastic precursor decay.[18] Formally, the principal difference in the two treatments is that the function F in Equation (10) and (14) is here related to chemical reaction kinetics rather than the dynamic elastic-plastic properties studied in Reference 18.

EXAMPLES

The capabilities of the model were assessed by the computation of examples of the initiation and detonation properties of several material-variations of TATB-based explosives. We determined the burning velocity parameters Z_B and T_B from the sustained-shock buildup curve from gauge data on 1.8-g/cm^3 (7% porous), "superfine" granular TATB,[16] and then used this burn velocity calibration for all the subsequent modeling of TATB-based explosives. A grain-size dimension $b = 0.02$ mm and a burning topology specified by $P_1 = 50$ GPa were used to represent the superfine TATB. Trial values of T_B and Z_B for the calibration were chosen such that their linear Arrhenius plots ($\ln V$ vs $1/T_B$) passed through a common high pressure point that reproduced the proper characterization of reaction zone for a steady detonation.[15] "Experimental" pressure histories from Reference 16 are shown in Figure 3; the first six of the profiles are fitted to Manganin-gauge data and the subsequent records are calculated with a DAGMAR rate form demonstrated to give detonation reaction-zone structures agreeing with interface velocimetry observations.[17] The upper dotted curve indicates the SHIN calculation of the shock-front locus the lower dotted curve the full reaction locus, the large dot signifies the run time to detonation – arbitrarily chosen where the shock front attains CJ pressure – and the inset label indicates the same information for the run to detonation (RTD) distance. These calculation were with $Z_B = 10.7$ mm and $T_B = 3800$ K. The front buildup history is in good agreement with both the gauge observations and the results of explosives wedge experiments. Gauge-pressure histories from the SHIN calculation are shown in Figure 4, along with the front buildup histories for three other choices of T_B. The values of Z_B for the four different temperature are 9.4, 10.3, 11.0 and 12.0. The results are seen to be quite sensitive to the choice of the parameter set (Z_B, T_B), and the gauge data discriminate well among different choices that all gave a proper reaction zone.

The rate calibration specified above was tested in SHIN calculations using different input shock strengths and was found to give excellent agreement with the

plot data (RTD vs input pressure) from explosives-wedge experiments.[16]

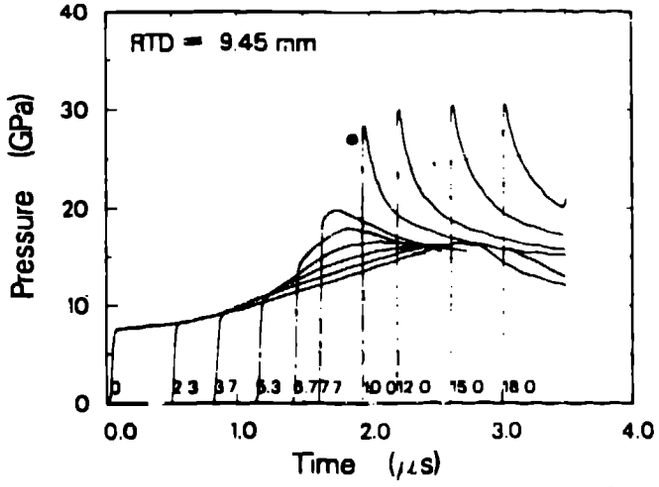

FIGURE 3. PRESSURE HISTORIES FOR 1.8-G/CM³ GRANULAR TATB IN A GAS-GUN EXPERIMENT. LABELS ON CURVES INDICATE GAUGE DISTANCE FROM THE IMPACT FACE, IN MILLIMETERS.

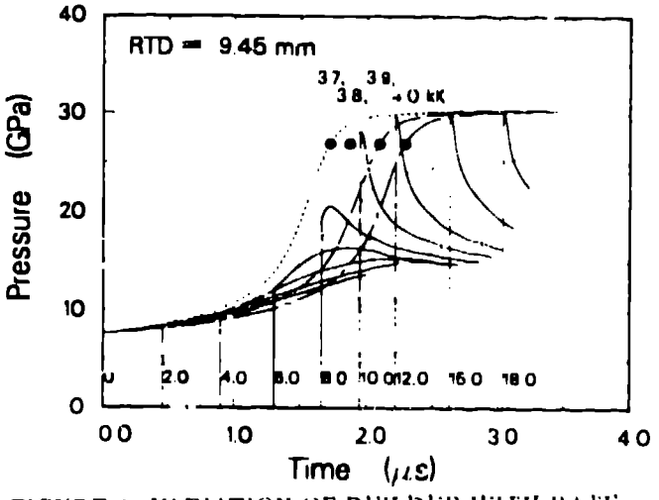

FIGURE 4. VARIATION OF BUILDUP WITH RATE CONSTANTS T_B AND Z_B FOR 1.8 G/CM³ TATB. UPPER LABELS INDICATE T_B VALUES.

The rate calibration described above was entirely with sustained-shock data, but short-shock data are known to provide much more stringent tests of reaction-rate models and were used in SHIN calculations of test examples. In Figure 5 we show pressure histories for a 10 GPa shock of 0.2 μs duration into the explosive. We see the buildup curve first rising, then falling and then rising again to detonation. Although the calculation did not have the same input as a specific experiment, the front and "gauge" pressure histories are both quite comparable to those reported in Reference 16. The run to detonation versus shock duration is shown in Figure 6. These calculations emphasize how sensitive the buildup process is to shock duration, with the transition from failure to detonate to sustained shock behavior occurs within 0.1 μs. Such sensitive behavior is a well-known qualitative characteristic of TATB explosives,[16,19,20] and the calculations we present are in specific quantitative agreement with observations on 1.8-g/cm³ superfine TATB with electrically-driven, 0.5-mm, Mylar flyers (see Figure 10 in Reference 19).

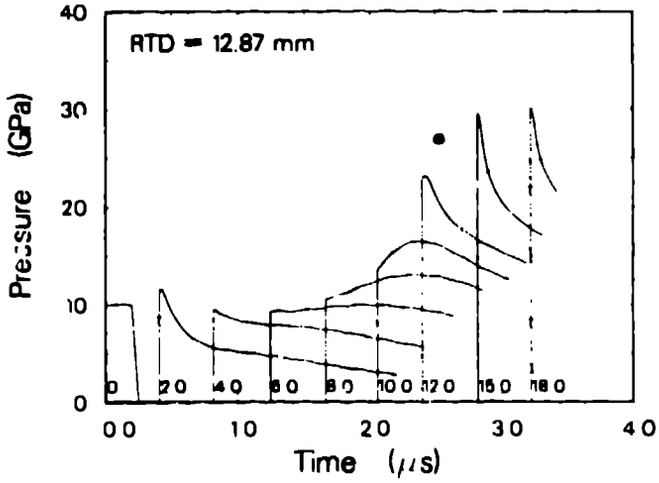

FIGURE 5. TYPICAL CALCULATION OF A SHORT SHOCK EXPERIMENT ON TATB.

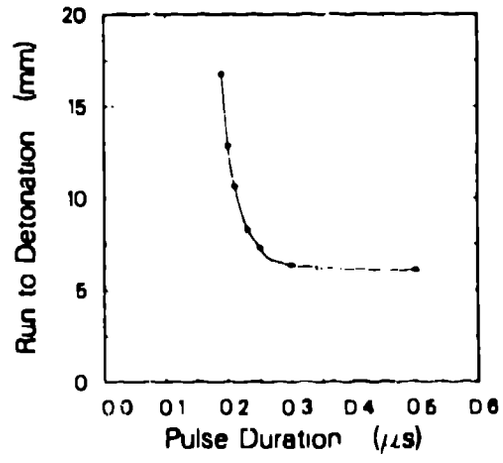

FIGURE 6. VARIATION OF RUN-TO-DETONATION DISTANCE WITH PULSE DURATION FOR 10 GPA SHORT SHOCKS INTO TATB.

Another example is for ramp loading. Pressure histories for a 0.5 μs ramp to 10 GPa are shown in Figure 7. We see that the shock builds up to 10 GPa at a depth of

about 5 mm. The remaining run distance of about 5 mm is only slightly less than the 6-mm RTD for a sustained, 10-GPa shock. This is so because little reaction starts before the shock reaches the 10-GPa level. Although we are unaware of any ramp-wave studies on TATB explosives, the suppression of reaction (commonly called desensitization) of the explosive by preshocking in complex geometries is well known.[21] With planar geometry, the plastic-bonded HMX, PBX 9404, displays extended run distances resembling those calculated here with both preshocks[8] and ramp-wave inputs.[22] This consequence of gradual loading is believed to result from the removal, or healing, of the density discontinuities that supply hot-spot sites. This phenomenon is simulated well by our surface-burning model because it depends strongly on the solid temperature, which in turn is significantly lower for isentropic, ramp-wave compression than for an equivalent-amplitude shock.

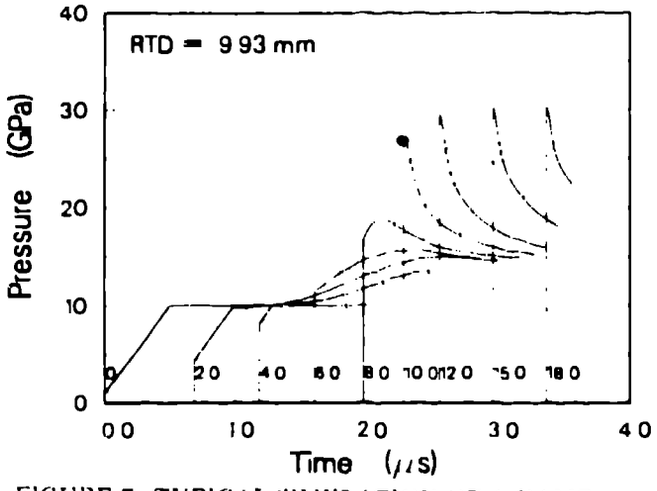

FIGURE 7. TYPICAL SIMULATION OF A RAMP LOADING EXPERIMENT ON 1.8 G/CM³ TATB.

One of the examples we did for multicomponent systems was for PBX 9502, a 1.89-g/cm³, 95/5 percent mixture of TATB and Kel-F 800. Pressure histories for the 10-GPa sustained shock are shown in Figure 8. The RTD obtained for several values of input pressures are shown on a Pop plot in Figure 9. On the same plot we show the experimental Pop plot obtained from wedge experiments.[10] We see that agreement is very good. Note that in this simulation we applied the rate parameters calibrated from the 1.8 g/cm³ pure TATB data as described above to TATB mixed with 5% inert binder, pressed to a much lower porosity (3.5% instead of 7%), and having a much higher RTD.

The multicomponent model was also applied to the study of the initiation properties of pure TATB explosives with a distribution of particle sizes. A parameter study of variations of these distributions about a common mean particle size demonstrated the mean value was the principal parameter in determining the buildup behavior.[4] An examination was made of the crossover in reaction rate observed for superfine and micronized TATB—specifically that in wedge experiments the relatively small-particle micronized TATB displays smaller RTD at higher (~20 GPa) input shock strengths and larger RTD at lower (~10 GPa) pressures than the superfine material.[20] To model this example, we found it necessary to impose the previously-mentioned requirement of a critical hot-spot size for ignition of the surface burn, and chose a critical size d_{cr} depending inversely on the exponent of the solid temperature. With this modification, the model gave excellent agreement with experiment. This result is detailed in Reference 5, and will not be discussed here.

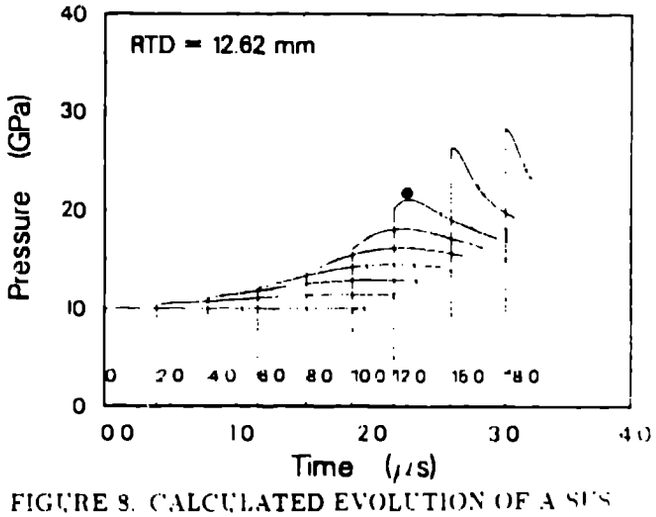

FIGURE 8. CALCULATED EVOLUTION OF A SUSTAINED SHOCK WAVE IN PBX 9502.

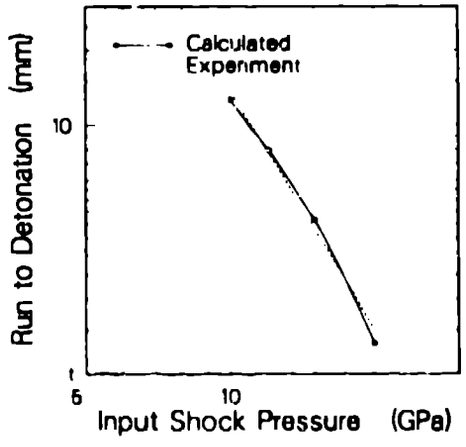

FIGURE 9. COMPARISON OF EXPERIMENTAL AND CALCULATED POP PLOTS FOR PBX 9

SUMMARY

We have developed a surface-burn model for shock initiation of solid explosives. It has been described in great detail in several reports and papers.[2-6] We applied it in a 1D, Lagrangian, method-of-characteristics hydrocode called SHIN and computed many examples. Several examples are presented in this paper.

In the reports we concentrated on detailed derivation of the equations and algorithms and detailed analysis of the computed results. Here we concentrate mainly on the outline of the *physical picture* behind the model. The essentials of the picture are:

- On the microscale (grain) level, initiation takes place through a two-stage process, ignition and growth. Ignition occurs at hot spots (or ignition sites) related to pores in the explosive.
- The ignition mechanism is through pore collapse and viscoplastic heating of pore boundaries. A few tens of nanoseconds after pressure is applied, the pore boundary material reacts, the cavity is filled with hot reaction products, and a hot spot is formed.
- The hot gas in the cavity drives into the unreacted solid a thin outgoing reaction zone. This moving burn surface is driven by heat conduction and fed by the heat of reaction.
- When threshold conditions for the cavity are met the moving burn surface attains a steady velocity that depends on the temperature of the solid ahead of it but not on the temperature of the gas behind.
- The hot-spot threshold conditions are a critical temperature, typically above 2500 K, and a critical hot-spot cavity size, which also depends on the solid temperature. Usually a cavity size above 1 μm is needed for weak shocks, and a size above 0.1 μm is sufficient for strong shocks.
- The burn-surface velocity dependence on solid temperature can be described by an Arrhenius relation with an activation temperature of the order of 5000 K. Calibration of reaction rate from experimental data includes determination of parameters in this Arrhenius relation.
- As the topology of the moving burn surfaces is complex and hard to determine, it is described by a burn-topology-function (BTF) with parameters calibrated from experimental data.
- The surface-burn model can be extended to multicomponent materials by using two approximations, a common average equation of state, and no interaction among the components in terms of one affecting the BTF of others.

Through the special case of steady detonation, we were able to show that, at least for TATB, surface burn is the overriding reaction process, and bulk reaction between the moving burn surfaces can be safely neglected.

By applying the surface-burn model to various situations, we conclude that it has a wide range of prediction capability. More work of comparisons with the results of critical experiments is, of course, needed.

REFERENCES

1. Bordzilovskii, S. A., et al., "Modeling the Shock Initiation of Detonation in Heterogeneous Explosives," Combustion, Explosion, and Shock Waves, Vol. 23, No. 5, 1988, p. 684 (English Translation of Fizika Godeniya Vzryva, 1987).
2. Partom, Y., "A Void Collapse Model for Shock Initiation," in Proceedings Seventh Symposium (International) on Detonation, NSWC MP 82-334, Annapolis, Maryland, June 16–19, 1981, pp. 506–516.
3. Partom, Y., Characteristics Code for Shock Initiation, Los Alamos National Laboratory report LA-10773, October, 1986, Los Alamos, New Mexico.
4. Partom, Y., Shock Initiation Modeling of Multi-Component Explosives, Los Alamos National Laboratory report LA-10773-Addendum, in press, Los Alamos, New Mexico.
5. Partom, Y., "Modeling the Crossover in Reaction Rate for Micronized TATB," in Shock Waves in Condensed Matter—1987 North Holland, Amsterdam 1988, pp. 535–538.
6. Partom, Y., The Shell Model for Hot-Spot Ignition, Los Alamos National Laboratory report LA-10874, 1987, Los Alamos, New Mexico.
7. Carroll, M. M., et al., "Application of a New Theory for the Pressure Induced Collapse of Pores in Ductile Materials," Proceedings of the International Symposium on Pore Structure on the Properties of Materials, Prague, 1973, pp.
8. Wackerle, J. D. and Anderson, A. B., "On the Shock Initiation of Heterogeneous Explosives," in the Topical Conference on Shock Waves in Condensed Matter, Pullman, Washington, June 1979. Available as Los Alamos National Laboratory informal report LA-UR-79-433, 1979.
9. Khasainov, et al., "Two Phase Visco-Plastic Model of Shock Initiation of Detonation in High Density Pressed Explosives," in Proceedings Seventh Symposium (International) on Detonation, NSWC MP 82-334, Annapolis, Maryland, June 16–19, 1981, pp. 435–444.
10. Frey, R. B., "Cavity Collapse in Energetic Materials," in Proceedings of the Eighth Symposium (International) on Detonation, NSWC MP 86-194, Albuquerque, New Mexico, July 15–19, 1985, pp. 68–80.
11. Kim, K. and Sohn, C. H., "Modeling of Reaction Buildup Processes in Shocked Porous Explosives," Ibid. pp. 926–933.
12. Nutt, G. L., "A Reactive Flow Model for a Monomolecular High Explosive," Journal of Applied Physics, Vol. 64, No. 4, 1988, p. 1815.
13. Wackerle, J. D. and Anderson, A. B., "Burning Topology in the Shock Induced Reaction of

Heterogeneous Explosives" in Shock Waves in Condensed Matter—1983, North-Holland, Amsterdam, 1984, pp. 601–604.
14. Mader, C. L., Numerical Modeling of Detonation, University of California Press, Berkeley, California, 1979, Appendix A.
15. Seitz, W. L., et al., "Detonation Reaction Zone Studies on TATB Explosives," in Proceedings of the Eighth Symposium (International) on Detonation, NSWC MP 86-194, Albuquerque, New Mexico, July 15–19, 1985, pp. 123–132.
16. Anderson, A. B., et al., "Shock Initiation of Porous TATB," in Proceedings Seventh Symposium (International) on Detonation, NSWC MP 82-334, Annapolis, Maryland, June 16–19, 1981, pp. 385–392.
17. Fickett, W. and Davis, W. C., Detonation, University of California Press, Berkeley, California, 1979, Section 4A.
18. Partom, Y., "Elastic Precursor Decay Calculation," Journal of Applied Physics, Vol. 59, No. 8, p. 2716.
19. Honodel, C. A., et al., "Shock Initiation of TATB Formulations" in Proceedings Seventh Symposium on Detonation, NSWC MP 82-334, Annapolis, Maryland, June 16–19, 1981, pp. 425–434.
20. Seitz, W. L., "Short-Duration Shock Initiation of Triaminotrinitrobenzene (TATB)" in Shock Waves in Condensed Matter—1983, North-Holland, Amsterdam, 1984, pp. 531–534.
21. Mader, C. L., "Explosive Desensitization by Preshocking" in 1972 International Conference on Combustion and Detonation Processess, Karlsruhe, Germany, June 27-29, 1979.
22. Setchell, R. E., "Ramp-Wave Initiation of Granular Explosives," Combustion and Flame, Volume 43, No. 3, p. 255 (1981).